A Free-Lagrange Simulation of Cavitation Bubble Collapse Near a Rigid Boundary

Cary K. Turangan and Graham J. Ball

School of Engineering Sciences, University of Southampton, Southampton SO17 1BJ, UK

Abstract. A numerical simulation of single cavitation bubble collapse near a rigid boundary is performed using a Free-Lagrange CFD code, assuming that the fluid motion is axisymmetric. The simulation is similar to an underwater explosion or laser- or spark-generated cavitation bubble, where the bubble grows to a maximum size due to a high initial pressure and later collapses. The stand-off parameter ξ is 1.19. During the collapse phase, the bubble migrates towards the rigid boundary and appears to elongate. Near the final stage of the collapse, the far side of the bubble involutes to form a high-speed microjet that penetrates the bubble. The impact of the jet onto the other side of the bubble produces a spherical blast wave, and the bubble becomes toroidal after the impact.

1 Introduction

It is well known that when cavitation bubbles collapse in the vicinity of a solid boundary (asymmetric collapse), complex and potentially destructive phenomena take place, including bubble elongation, high-speed microjets that penetrate the bubble towards the solid boundary as well as shock wave emissions. Intensive studies regarding these phenomena have been carried out in the past with experiments, theoretical investigations and numerical simulations because of their relevance to initiation of explosives, surface pitting and erosion in fluid machinery, sonoluminescene, medical lithotripsy, etc..

In experimental investigations, the optical cavitation technique, in which a laser beam is focused into water to create a vapour bubble, has become popular [4–6]. This is because it allows the generation of the bubbles under controlled conditions including location, time, size and number. High-speed photography has revealed most of the events associated with asymmetric cavitation collapse, i.e. bubble elongation, liquid-jet formation and shock wave emissions [4,5,8].

The dynamic behaviour of the bubble and the damage patterns caused by the collapse have been found to be strongly dependent on the non-dimensional stand-off parameter ξ. This is defined as the ratio of the initial distance of the bubble centre to the wall, d, to the maximum bubble radius R_m. Although experimental diagnostics are able to show the key events of asymmetric cavitation bubble collapse, understanding of these process is incomplete due to limited temporal and spatial resolution.

Numerical simulations have the potential to provide an improved understanding of cavitation bubble dynamics, but they are difficult to perform with conventional CFD methods because of the need to accurately track the air/water

interface. Numerical simulations using the Boundary Integral Method agree well with experimental results, including the jet formation but are limited to events with weak shocks [6,9]. The method is over-restrictive for general application due to the assumptions that the liquid is incompressible, irrotational and that the gas scalar properties are spatially uniform.

Numerical simulations using Lagrangian methods offer a significant advantage in simulating multi-fluid flows, such as the cavitation bubble collapse, because of the Lagrangian formulation, in which the mesh convects with the local flow velocity. As a result, material interfaces are sharply resolved and numerical diffusion is minimised for convecting structure [3]. However, conventional Lagrangian schemes that use fixed-connectivity meshes are unable to simulate flows with high material deformation due to excessive mesh distortion and entanglement. The Free-Lagrange (FL) method [1], while retaining the benefits of the Lagrangian formulation, overcomes problems of mesh entanglement because the mesh connectivity is allowed to evolve naturally.

The main objective of the present work is to simulate the growth and collapse of a single generic cavitation bubble near a plane rigid boundary using the Free-Lagrange method in axisymmetric form.

2 Numerical Method

The Free-Lagrange CFD code *Vucalm*, developed by Ball [1], solves the unsteady, inviscid and compressible Euler equations in the axisymmetric Lagrangian reference frame and in finite volume form. A simple interface smoothing algorithm [2,3] is utilised in order to overcome the mesh-induced high wave number wrinkling at material interfaces that is common in Free-Lagrange schemes.

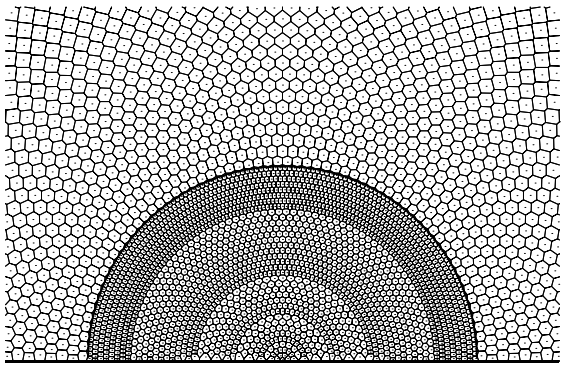

Fig. 1. Initial Voronoi mesh used in the Free-Lagrange simulation. Semi-circular solid line represents material interface and dots indicate positions of fluid particles.

At the start of calculation, the computational domain is filled with computational 'particles', and associated with each particle is a fluid type and properties,

coordinates and flow conditions. A Voronoi diagram is constructed based on the particle positions to form polygonal cells that enclose each particle (Fig. 1). The mass for each cell remains constant throughout the calculation and mass exchange between particles is forbidden. Therefore mass conservation is automatically satisfied.

The flow solvers are of Godunov-type and nominal second order spatial accuracy is achieved using a piece-wise linear reconstruction of flow variables. To ensure monotonicity at steep gradients, a MUSCL-based slope limiter is used. The integration of the governing equations is explicit first-order accurate in time. In the current work, the HLLC approximate Riemann solver is used at gas/gas cell boundaries and an exact solver [12] at gas/water and water/water boundaries.

3 Problem Specification

The generic cavitation bubble simulated here resembles an underwater explosion or laser-generated bubble, in which the high initial pressure within the gas bubble causes it to expand. When the gas pressure has dropped well below the ambient pressure, the expansion is halted and the bubble starts to collapse.

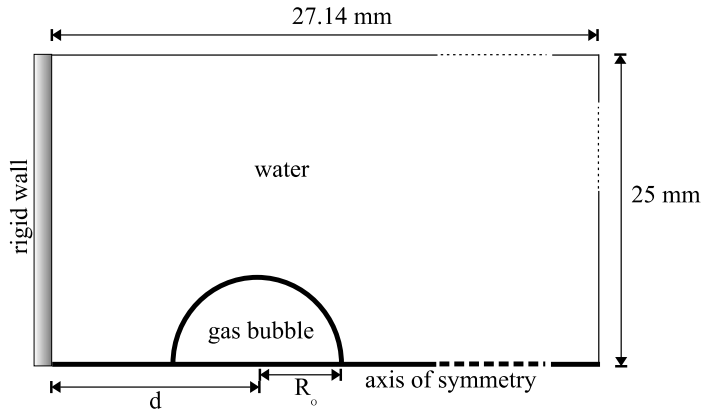

Fig. 2. Schematic diagram of the computational domain

The schematic diagram of the computational domain is shown in Fig. 2. The left and bottom computational boundaries represent the rigid wall and the axis of symmetry respectively. For computational convenience, the top and right boundaries are also fully reflecting solid boundaries. Therefore, the pressure waves emitted by the bubble at the initiation and the collapse will be reflected back into the domain. Although these wave reflections, particularly from the initial shock wave, may cause a slight decrease in oscillation period, they do not produce any significant modification in the dynamics of the bubble [7].

At the initiation of the calculation, the gas bubble has an initial radius R_o of $0.229\,mm$, and the centre of the bubble is located $2.14\,mm$ away from the rigid wall. The gas is modeled as air, and is represented by the ideal gas Equation of State (EOS). The initial density, pressure and temperature in the gas bubble are $81.06\,MPa$, $97.34\,kgm^{-3}$, and $2900\,K$ respectively. The water is represented by the Tait EOS and is initially at ISA sea level conditions, i.e. the density, pressure and temperature are $1000\,kgm^{-3}$, $0.101\,MPa$ and $288.15\,K$ respectively .

4 Results and Discussion

Following flow initialisation, a spherical shock is emitted into the water, while an expansion wave moves towards the centre of the bubble. Fig. 3 shows the pressure-time history at a recording point close to the rigid wall on the symmetry axis. As the shock front reaches the recording point, the magnitude of the pressure has dropped to about $17\,MPa$, as indicated by the first spike in Fig. 3. The initial shock is reflected back into the domain by the rigid wall and causes the bubble to migrate slightly away from the wall.

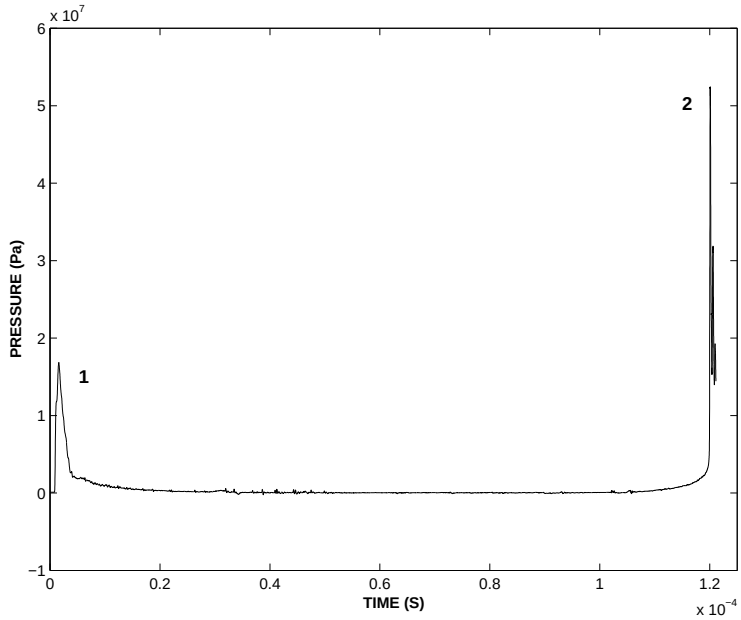

Fig. 3. Pressure-time history on axis, $0.31\,mm$ from the rigid boundary. Pressure events: (1)initial shock emitted by bubble; (2)blast wave due to severing of bubble by liquid microjet.

Fig. 4-6 show the velocity field at various stages during the evolution of the flow; the velocity vector scaling has been selected in each figure to highlight the flow structure, and is not the same at each stage.

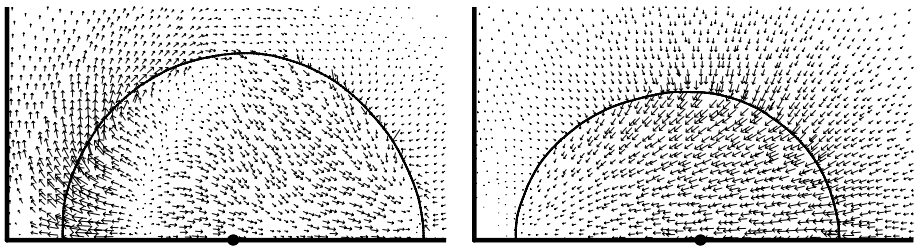

(a) $t = 59\,\mu s$ (b) $t = 93\,\mu s$

Fig. 4. Velocity vectors: (a)Bubble at maximum size, and (b)Bubble elongates. Note that the dot on the axis of symmetry indicates the initial location of the bubble centre.

The bubble reaches maximum radius R_m of $1.8\,mm$ at $t \approx 59\,\mu s$ (Fig. 4a), hence $R_m/R_o = 7.86$. At this time, the pressure of the gas inside the bubble varies from approximately $42\,kPa$ in the centre, to $45\,kPa$ near the interface. As this gas pressure is well below the static ambient pressure, the expansion is halted and the bubble starts to collapse. The presence of the rigid wall destroys the symmetry of the fluid flow and strongly influences the evolution of the bubble interface.

As shown in Fig. 4a, the left bubble interface still moves towards the wall due to the inertia of the expansion, whereas the top and right interfaces have started to contract as the surrounding water accelerates inwards. Consequently, the bubble migrates towards the rigid wall and later appears to elongate (Fig. 4b).

The migration of collapsing bubbles towards solid boundaries is a phenomenon of asymmetric collapse which has been observed experimentally [4,8] as well as numerically [6,9]. It is believed that this phenomenon increases the damage capability [4] of the bubble collapse because the effects of shock wave emissions and microjets are more pronounced on the solid boundaries as the distance to the wall is reduced.

In Fig. 4b, at time $t = 93\,\mu s$, the water between the bubble and the rigid wall appears to stagnate while elsewhere the predominant fluid motion is convergent towards the wall and the symmetry axis. In addition, the contraction of the bubble interface becomes more significant and the right interface has been slightly flattened.

Subsequently, the right interface involutes to form a high-speed microjet that is directed towards the rigid wall. At time $t = 117\,\mu s$ (Fig. 5a), the jet has penetrated about half of the bubble, and by $t = 119.1\,\mu s$ (Fig. 5b) the jet has

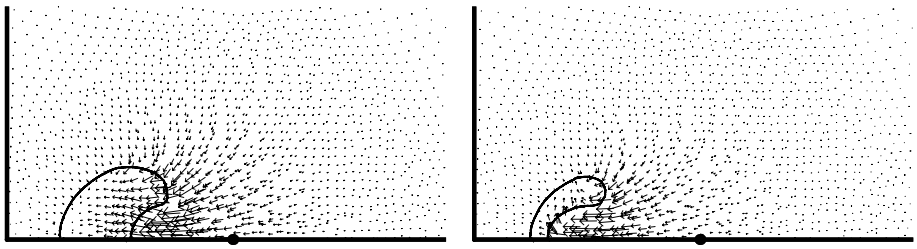

(a) $t = 117\,\mu s$ (b) $t = 119.1\,\mu s$

Fig. 5. High-speed microjet penetrating the bubble

accelerated to approximately $240\,m/s$. During this time, the gas between the left interface and the jet tip is compressed and later causes the velocity of the jet to decrease as it approaches the left interface.

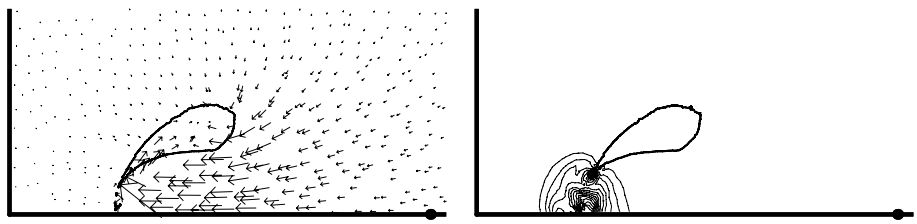

(a) $t = 119.93\,\mu s$ (b) $t = 120.01\,\mu s$

Fig. 6. Close-up of the bubble: (a)microjet strikes the left bubble interface, (b)blast wave produced by the impact of the jet; contours of pressure, $\Delta P = 15\,MPa$

A liquid-liquid impact takes place when the high-speed microjet, with a tip diameter of approximately $0.2\,mm$, hits the left interface, where the point of impact is $0.54\,mm$ away from the rigid wall (Fig. 6a). The tip velocity has decreased to about $215\,m/s$. The impact produces a blast wave (Fig. 6b), in which the peak pressure in the core of the impact reaches approximately 2.5 times the pressure at initiation. The second spike in Fig. 3 indicates the pressure rise due to this impact. It also leads to the creation of new micro-bubbles from the gas layer trapped between the jet and the left interface [2]. After impact, the velocity of the jet tip falls, and as the jet moves towards the rigid wall, a ring vortex is created which interacts with the bubble.

The blast wave emitted by the liquid-liquid impact is found to generate negative pressure (tension) in the water behind the jet (in the jet funnel). The magnitude of this negative pressure is higher than the limiting value, so that spontaneous secondary cavitation is expected to occur here, although this mechanism is not modeled in the present simulation. This observation supports the suggestion of Ohl. et al [11] that this secondary cavitation forms the 'counter-jet'.

The sequence of physical events from the current simulation, is similar to those observed in experiments [4,6,8,9,11] and other numerical simulations [6,9].

5 Conclusion

The simulation of the growth and collapse of a single cavitation bubble near a rigid boundary in an axisymmetric environment has been performed using the Free-Lagrange code *Vucalm*. The results show the ability of the method to capture the physical phenomena of bubble elongation and jet formation, as well as shock wave emission due to the impact of the jet. The jet reaches a peak velocity of about $240\,m/s$. However, as the jet is approaching the other side of the bubble, the compressed gas in between causes the jet to decelerate somewhat prior to impact. A spherical blast wave is emitted into the surrounding as a result of the liquid-liquid impact and the bubble becomes toroidal after the jet has pierced the bubble. In addition, the impact has potential to cause the generation of new micro-bubbles from the gas layer that is trapped between the water and the jet tip. Negative pressure sufficient to cause spontaneous secondary cavitation is generated behind the jet tip after impact. In conclusion, the results agree qualitatively well with experiments as well as with other numerical models. Further work will cover various stand-off parameters and the replacement of the rigid wall with an elastic/plastic material model.

References

1. Ball GJ (1996) A Free-Lagrange method for unsteady compressible flow: simulation of a confined cylindrical blast wave. Shock Waves 5:311–325
2. Ball GJ, Howell BP, Leighton TJ, Schofield MJ (2000) Shock-induced collapse of a cylindrical air cavity in water: a Free-Lagrange simulation. Shock Waves 10:265–276
3. Howell BP, Ball GJ (2000) Damping of mesh-induced in Free-Lagrange simulations of Richtmyer-Meshkov instability. Shock Waves 10:253–264
4. Philipp A, Lauterborn W (1998) Cavitation erosion by single laser-produced bubbles. J Fluid Mech 361:75–116
5. Isselin JC, Alloncle AP, Autric M (1998) On laser induced single bubble near a solid boundary: Contribution to the understanding of erosion phenomena. J Appl Phys 84:5766–5771
6. Tong RP, Schiffers WP, Shaw SJ, Blake JR, Emmony DC (1999) The role of 'splashing' in the collapse of a laser-generated cavity near a rigid boundary. J Fluid Mech 380:339–361
7. Menon S, Lal M (1998) On the dynamics and instability of bubbles formed during underwater explosions. Exp Thermal and Fluid Science 16:305–321

8. Tomita Y, Shima A (1986) Mechanisms of impulsive pressure generation and damage pit formation by bubble collapse. J Fluid Mech 169:535–564
9. Zhang S, Duncan JH, Chahine GL (1993) The final stage of the collapse of a cavitation bubble near a rigid wall. J Fluid Mech 257:147–181
10. Noack J, Hammer DX, Noojin GD, Rockwell BA, Vogel A (1998) Influence of pulse duration on mechanical effects after laser-induced breakdown in water. J Appl Phys 83:7488–7495
11. Ohl CD, Kurz T, Geisler R, Lindau O, Lauterborn W (1999) Bubble dynamics, shock waves and sonoluminescene. Phil Trans R Soc Lond A 357:269–294
12. Flores J, Holt M (1981) Glimm's method applied to underwater explosions. J Comp Phys 44:377–387